Published in "The Plant Journal 77(1): 108–118, 2014"
which should be cited to refer to this work.

Expression of TWISTED DWARF1 lacking its in-plane membrane anchor leads to increased cell elongation and hypermorphic growth

Aurélien Bailly[1,2,†], Bangjun Wang[1,2,3,‡], Marta Zwiewka[4,7], Stephan Pollmann[5,§], Daniel Schenck[6], Hartwig Lüthen[6], Alexander Schulz[3], Jiri Friml[4,7,8] and Markus Geisler[1,2,*]

[1]*Department of Biology – Plant Biology, University of Fribourg, Fribourg, Switzerland,*
[2]*Institute of Plant Biology, University of Zurich, Zurich, Switzerland,*
[3]*Department of Plant and Environmental Sciences, University of Copenhagen, Frederiksberg, Denmark,*
[4]*Mendel Centre for Plant Genomics and Proteomics, Central European Institute of Technology (CEITEC), Masaryk University (MU), Brno, Czech Republic,*
[5]*Ruhr-Universität Bochum, Lehrstuhl für Pflanzenphysiologie, Germany,*
[6]*Biozentrum Klein Flottbek, Universität Hamburg, Hamburg, Germany,*
[7]*Department of Plant Systems Biology, VIB and Department of Plant Biotechnology and Bioinformatics, Ghent University, Gent, Belgium, and*
[8]*Institute of Science and Technology (IST) Austria, Klosterneuburg, Austria*

*For correspondence (e-mail markus.geisler@unifr.ch).
[†]Present address: Institute for Plant Biology, Department of Microbiology, University of Zurich, 8008 Zurich, Switzerland.
[‡]Present address: School of Life Sciences, Southwest University, Chongqing 400715, China.
[§]Present address: Centro de Biotecnología y Genomica de Plantas, Campus de Montegancedo, 28223 Pozuelo de Alarcón, Madrid, Spain.

SUMMARY

Plant growth is achieved predominantly by cellular elongation, which is thought to be controlled on several levels by apoplastic auxin. Auxin export into the apoplast is achieved by plasma membrane efflux catalysts of the PIN-FORMED (PIN) and ATP-binding cassette protein subfamily B/phosphor-glycoprotein (ABCB/PGP) classes; the latter were shown to depend on interaction with the FKBP42, TWISTED DWARF1 (TWD1). Here by using a transgenic approach in combination with phenotypical, biochemical and cell biological analyses we demonstrate the importance of a putative C-terminal in-plane membrane anchor of TWD1 in the regulation of ABCB-mediated auxin transport. In contrast with dwarfed *twd1* loss-of-function alleles, *TWD1* gain-of-function lines that lack a putative in-plane membrane anchor (HA–TWD1-C_t) show hypermorphic plant architecture, characterized by enhanced stem length and leaf surface but reduced shoot branching. Greater hypocotyl length is the result of enhanced cell elongation that correlates with reduced polar auxin transport capacity for HA–TWD1-C_t. As a consequence, HA–TWD1-C_t displays higher hypocotyl auxin accumulation, which is shown to result in elevated auxin-induced cell elongation rates. Our data highlight the importance of C-terminal membrane anchoring for TWD1 action, which is required for specific regulation of ABCB-mediated auxin transport. These data support a model in which TWD1 controls lateral ABCB1-mediated export into the apoplast, which is required for auxin-mediated cell elongation.

Keywords: polar auxin transport, ABCB, P-glycoprotein, TWISTED DWARF1, cell elongation.

INTRODUCTION

The success of modern land plants relies on the ability to collect sufficient light for photosynthesis, which is accomplished by the formation of tall plant architecture (Hager, 2003). This architecture is mainly achieved by cell elongation against a stretchable cell wall that, dependent upon the specific tissue, results in axial elongation or lateral expansion (Bennett and Scheres, 2010). According to the acid growth theory (Rayle and Cleland, 1970), the plant signaling molecule auxin promotes elongation of cells by stimulating proton extrusion into the apoplast. The apoplastic fraction of auxin-binding protein1, ABP1, located at the outer surface of the plasma membrane (PM) has been demonstrated to function as an auxin receptor during auxin-controlled cell elongation (Braun *et al.*, 2008).

Conversely, the auxin-efflux transporter complex itself has also been suggested as a candidate receptor (Zhao *et al.*, 2002; Hossel *et al.*, 2005). However, the recent finding that rapid, auxin-induced hypocotyl elongation is not significantly affected in a quadruple TIR1/AFB mutant provides evidence that transcriptional up-regulation is not essential at least for the early phase (<30 min) of this process (Schenck *et al.*, 2010).

However, up to now it is unclear how an apoplastic auxin receptor attached to the PM surface is connected to intercellular auxin gradients that are generated by the cell-to-cell transport of auxin, a process that is designated as polar auxin transport (PAT; reviewed in Robert and Friml, 2009; Vanneste and Friml, 2009). Due to the chemical properties of the major relevant auxin, indolyl acetic acid (IAA), PAT is controlled on the efflux level catalysed by members of the PIN (PIN-FORMED) and B subfamily of ABC transporters, called ABCBs/PGPs/multidrug resistances (MDRs) (Geisler and Murphy, 2006).

Multilaterally expressed ABCBs are thought to minimize apoplastic auxin reflux by pumping against steep PM auxin gradients in tissues with high apoplastic auxin concentrations (Geisler and Murphy, 2006; Wang *et al.*, 2013). ABCB1/PGP1 was the first ABCB transporter demonstrated to catalyse the export of auxin (Geisler *et al.*, 2005; Geisler and Murphy, 2006), although an involvement in hypocotyl elongation was suggested long before (Sidler *et al.*, 1998). ABCB1 and ABCB19/PGP19/MDR1-mediated long-range transport of auxin has been shown to be dependent on physical interaction with the FKBP42 (FK506-binding protein), TWISTED DWARF1 (TWD1), which is documented by a close overlap between *twd1* and *abcb1abcb19* dwarf phenotypes and undirected helical disorientation of growth at later stages (Geisler *et al.*, 2003; Bouchard *et al.*, 2006; Geisler and Bailly, 2007; Bailly *et al.*, 2008; Henrichs *et al.*, 2012). Recently, it has been demonstrated that TWD1 functions in recruitment of the AGC kinase, PINOID, shown to phosphorylate the ABCB1 linker leading to altered ABCB1 auxin transport capacities (Henrichs *et al.*, 2012; Geisler and Henrichs, 2013). Conversely, plasma membrane ABCB isoforms B1, B4 and B19 were found to be delocalized on the endoplasmic reticulum (ER) and strongly degraded in *twd1*, a finding that suggests that TWD1 has both an effect on ABCB activity as well as on its targeting and stability (Wu *et al.*, 2010; Wang *et al.*, 2013).

Using a wide range of methods and constructs, TWD1 has been localized independently to several membrane locations, including the PM, the tonoplast and the ER (Kamphausen *et al.*, 2002; Geisler *et al.*, 2003; Henrichs *et al.*, 2012; Wang *et al.*, 2012, 2013). Remarkably, in the root epidermis TWD1 immunodecoration was most pronounced at lateral PM domains with stronger labeling at the outward-facing side, in line with their proposed function in preventing lateral apoplastic reflux (Wang *et al.*, 2013). TWD1 was originally thought to be membrane-bound via glycosylphosphatidyl-inositol (GPI) anchoring, which was based mainly on a low homology of its C-terminus to classical GPI moieties and its difficult solubilization by detergents (Geisler *et al.*, 2003). Nuclear magnetic resonance (NMR) data provided convincing evidence that TWD1 has a C-terminal in-plane membrane (IPM) anchor, however the relevance of membrane anchoring remains exclusive. Human FKBP38, the closest human TWD1 ortholog, acts as a negative regulator of apoptosis (Shirane and Nakayama, 2003) and a positive regulator of plasma membrane ion channel biogenesis (Banasavadi-Siddegowda *et al.*, 2011). Absence of its membrane anchor leads to mistargeting of FKBP38 and subsequent apoptosis (Shirane and Nakayama, 2003) but increases cystic fibrosis conductance regulator (CFTR) synthesis (Banasavadi-Siddegowda *et al.*, 2011).

Here we present a *TWD1* gain-of-function allele that lacks the putative C-terminal IPM anchor (HA–TWD1-C_t). *HA–TWD1-C_t* lines display a hypermorphic plant architecture, characterized by enhanced stem length and leaf surface but reduced shoot branching. Greater shoot sizes are caused by enhanced cell elongation, which correlates with reduced polar auxin transport capacities for HA–TWD1-C_t, and which results in elevated auxin levels and auxin-induced cell elongation rates in the hypocotyl. Our data provide further evidence on the function of IPM anchoring of the FKBP42, TWD1, and support a model in which auxin export provided by the TWD1/ABCB1 complex alters lateral, apoplastic concentrations required for auxin-mediated cell elongation.

RESULTS

Expression of TWD1 lacking its C-terminal membrane anchor results in hypermorphic plants

In order to better understand the importance of IPM anchoring of TWD1 and its role in ABCB regulation we have functionally complemented the *twd1-3* allele by introducing an HA-tagged, truncated version that lacks the C-terminal IPM anchor (amino acid residues 338–365) expressed under the control of the constitutive CaMV 35S promoter. While the full-length version of TWD1 (HA–TWD1) complemented the 'twisted dwarf syndrome' in all aspects to wild-type level (Geisler *et al.*, 2003; Bouchard *et al.*, 2006; Figure 1, Tables S1 and S2), all independent lines that expressed the truncated version (HA–TWD1-C_t) showed a severe hypermorphic phenotype, most obviously characterized by drastically enhanced stem length, stem diameter and leaf surface [Figures 1(a–c) and S1].

A detailed comparison of phenotypic and developmental stages (Boyes *et al.*, 2001) of *twd1-3*, HA–TWD1 and HA–TWD1-C_t alleles revealed no significant differences with wild-type up to cotyledon stages, but a significant

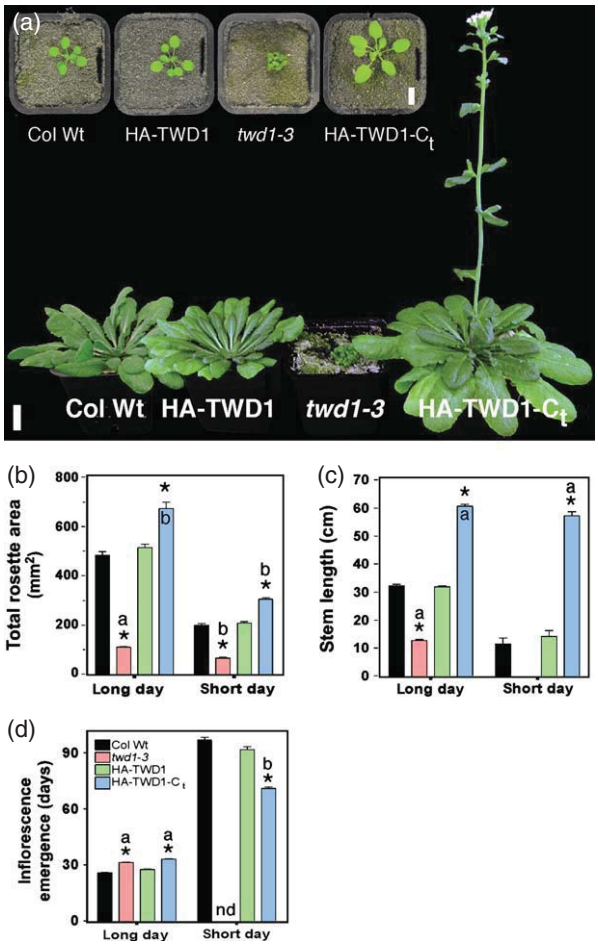

Figure 1. Expression of HA–TWD1-C_t results in hypermorphic plants characterized by enhanced stem length and leaf surface.
(a) Phenotypes at 70 days after germination (dag) and 10 dag (inset) pot-grown wild type (Col Wt) and *TWD1* loss-of-function (*twd1-3*) placed between gain-of-function lines with (HA–TWD1) and without C-terminal in-plane membrane anchor (HA–TWD1-C_t) grown under 8 h light cycle. Scale bars: 1 cm. (b–d) Total rosette area (b), stem lengths (c) and inflorescence emergence (d) of Wt (Col Wt), *twd1-3*, HA–TWD1 and HA–TWD1-C_t lines grown under indicated light conditions. nd; not determined; stem length in *twd1-3* under short-day conditions is '0'. For a detailed developmental analysis, see Tables S1 and S2. Mean ± standard error (SE); $n = 4$–10. Significant differences were determined by analysis of variance (ANOVA) using the Tukey test for multiple comparisons: $P < 0.01$ to Wt (b–d) are indicated by an asterisks.

effect on inflorescence emergence in *twd1-3* and HA–TWD1-C_t (Tables S1 and S2). An interesting finding was that under short-day light conditions (8 h light cycles) HA–TWD1-C_t showed an early-flowering phenotype, which was converted to late-flowering by long-day conditions (16 h light cycles) as found for *twd1-3* [Figure 1(d)]. However, the inflorescence emergence delay at 16 h light is compensated by an elongated life cycle for HA–TWD1-C_t. Therefore, independently of day length, manipulation of TWD1 expression levels resulted in highly reduced or enhanced final stem length and leaf area in *twd1-3* or HA–TWD1-C_t [Figure 1(b,c)], respectively. Total leaf surface in HA–TWD1-C_t is further enhanced by the fact that HA–TWD1-C_t produces a higher number of rosette leaves (Figure S1 and Table S2), a common trait of early-flowering mutants (Teper-Bamnolker and Samach, 2005).

An unexpected finding was that the greater stem lengths of HA–TWD1-C_t were accompanied by a drastic reduction of shoot branching [Figure 2(a,b)]. This outcome was also found for *twd1-3* but obviously at a lower magnitude [Figure 2(c)]. In contrast, however, analysis of inflorescence lengths revealed that hypermorphism of HA–TWD1-C_t was reached by a higher node number and a more equal distribution of inflorescence lengths at these nodes [Figure 2(c)]. The opposite was found for *twd1*, which was widely phenocopied by *abcb1 abcb19* stems [Figure 2(c)]. Additionally, branching also occurred in HA–TWD1-C_t but at a higher node numbers closer to the shoot tip [Figure 2(d)].

Branching defects argue for altered IAA concentrations (see below) that however might alter also shoot transport of strigolactone known to collectively control shoot branching (Gomez-Roldan *et al.*, 2008); analyses of the latter are underway.

Hypermorphic shoots in *HA–TWD1-C_t* are caused predominantly by IAA-controlled enhanced cell elongation

A quantification of hypocotyl lengths, used here as a marker for shoot development under different light fluencies revealed that hypocotyl length was strongly reduced in *twd1* in the light and in the dark but greatly enhanced in *HA–TWD1-C_t* in the presence of light [Figures 3(b) and S2], and in general is known to repress hypocotyl elongation (Jensen *et al.*, 1998). In contrast, root elongation in *twd1* is promoted in the dark but inhibited with increasing light intensities (Geisler *et al.*, 2003; Figure S2).

Analysis of hypocotyl cell length and cell numbers revealed that dwarfism/hypermorphism of *twd1*/*HA–TWD1-C_t* is caused predominantly by reduced/enhanced cell elongation and not by alterations in division [Figure 3(a–d)]. While the cell number remained constant [Figure 3(c)], hypocotyl cell length was significantly reduced/enhanced in *twd1*/*HA–TWD1-C_t*. Interestingly, most differences between wild-type and *TWD1* loss- or gain-of-function lines were light-dependent [reinforced with short-day (8 h light) compared with long-day conditions (16 h light)]. This finding is analogous to the late-flowering phenotypes of *abcb* mutants shown to be controlled directly by PAT (Geisler *et al.*, 2005).

In order to test if reduced/enhanced hypocotyl cell length in *twd1*/*HA–TWD1-C_t* was auxin-dependent, we quantified hypocotyl elongation after application of external IAA, an established test system for auxin-mediated shoot physiology (Schenck *et al.*, 2010). In agreement with

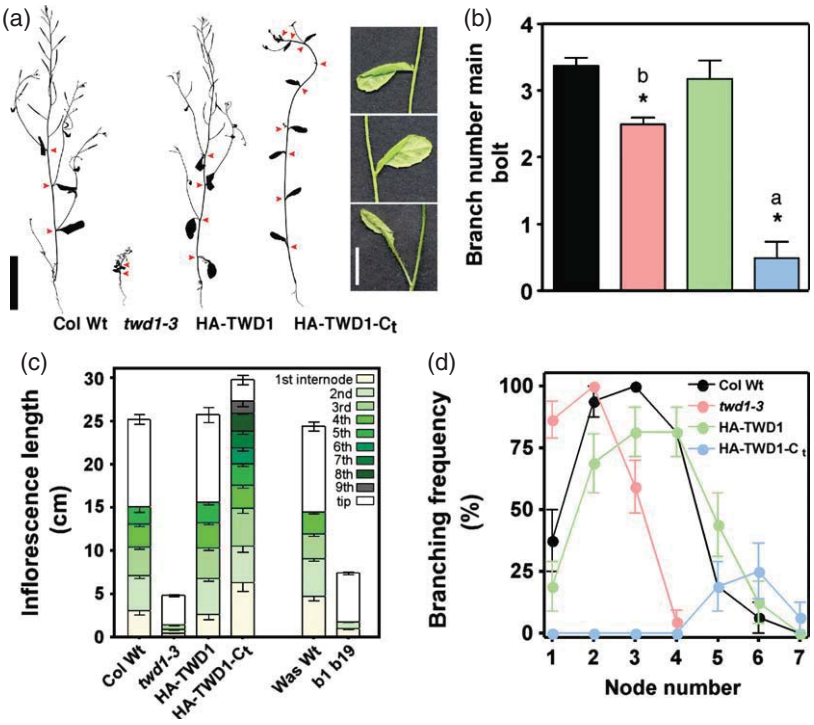

Figure 2. Shoot branching is highly reduced in HA–TWD1-C_t.
(a) Photographs of plants at 45 days after germination (dag): Wt (Col Wt), *twd1-3*, HA–TWD1 and HA–TWD1-C_t lines grown under 16 h light conditions. Scale bar: 2 cm. Inset, close-up pictures of first, second and third branching points, indicated by red arrows.
(b) Quantification of branch numbers of *twd1-3*, HA–TWD1, HA–TWD1-C_t and wild type (Col Wt) 40-day stems grown under 16 h light conditions. Mean ± standard error (SE); $n > 30$; legend as in D.
(c) Quantification of inflorescence lengths of *twd1-3*, HA–TWD1, HA–TWD1-C_t and wild type (Col Wt) 40-day stems grown under 16 h light conditions. Mean ± SE; $n > 30$.
(d) Relative branching per node of *twd1-3*, HA–TWD1, HA–TWD1-C_t and wild type (Col Wt) 40-day stems grown under 16 h light conditions. Mean ± SE; $n > 30$. Significant differences were determined by analysis of variance (ANOVA) using the Tukey test for multiple comparisons: (a) $P < 0.01$; (b) $P < 0.05$) to Wt controls are indicated by an asterisk.

hypocotyl cell length quantification, IAA induction of hypocotyl organ elongation was slightly, but significantly, reduced in *twd1* [104.7% ± 3.2 compared with 106.8 ± 1.6% of Columbia wild-type (Col Wt)] but drastically enhanced in HA–TWD1-C_t (113.9 ± 4.1%) and HA–TWD1 [115.1 ± 3.0%; Figure 3(e)].

In summary, these data suggest a role for TWD1 in determination of a wide range of late plant development (including hypocotyl elongation and floral transition) and physiological processes in an action known to be directly determined by PAT.

TWD1 gain-of-function results in enhanced cellular auxin efflux

Hypermorphic shoot phenotypes as well as enhanced hypocotyl cell elongation rates for *TWD1* gain-of-function lines that are dependent on the presence, quantity and day length of light argue for altered PAT capacities as underlying molecular mechanisms. Therefore we quantified transport of the native and synthetic auxins, IAA and 1-naphthaleneacetic acid (NAA), on the cellular as well as on the tissue/organ levels.

Using the well established leaf mesophyll protoplast system (Geisler *et al.*, 2005; Petrasek *et al.*, 2006), we found that, as with *abcb1 abcb19*, both *twd1* alleles showed reduced IAA export from single cells [*twd1-1*: 53.7 ± 6.4% of Wassilewskija (Was) Wt; *twd1-3*: 69.9 ± 16.0% of Col Wt; Figure 4(a)], and verified previous results for *twd1-1* (Bouchard *et al.*, 2006). However, both *TWD1* gain-of-function lines significantly export more IAA (HA–TWD1: 117.4 ± 9.6% and HA–TWD1-C_t: 138.5 ± 18.9% Wt) compared with the wild type. Significant up-regulation in TWD1-OX was to an even higher amount also found for NAA assayed in parallel but surprisingly not for both *twd1* alleles that export NAA to nearly wild-type levels [Figure 4(a)].

In order to investigate this interesting finding further we co-expressed ABCB1 and TWD1 in the yeast *Schizosaccharomyces pombe* allowing functional analyses of both B1 and B19 in the absence of plant-specific factors (Yang and Murphy, 2009). Analogous to co-expression of B1/TWD1 in mammalian HeLa cells (Bouchard *et al.*, 2006), TWD1 clearly up-regulated B1- and B19-mediated auxin export but had no significant effect on NAA export assayed in parallel [Figure 4(b)].

Auxin substrate selectivity was also found in baker's yeast, *Saccharomyces cerevisiae*, known to have – in comparison to the protoplast and *S. pombe* systems – an inhibitory impact on ABCB1-mediated IAA efflux (roughly 50%; Figure S3; Bouchard *et al.*, 2006). This finding has recently been shown to be caused by competition of TWD1 with the yeast endogenous FKBP, ScFKBP12, that is apparently highly competent in ABCB up-regulation (Bouchard *et al.*, 2006; Bailly *et al.*, 2008; Henrichs *et al.*, 2012). However, in this yeast system, TWD1 co-expression blocked ABCB1-mediated IAA efflux but did not have any significant inhibitory effect on the export of NAA or the diffusion control, benzoic acid (BA; Figure S4).

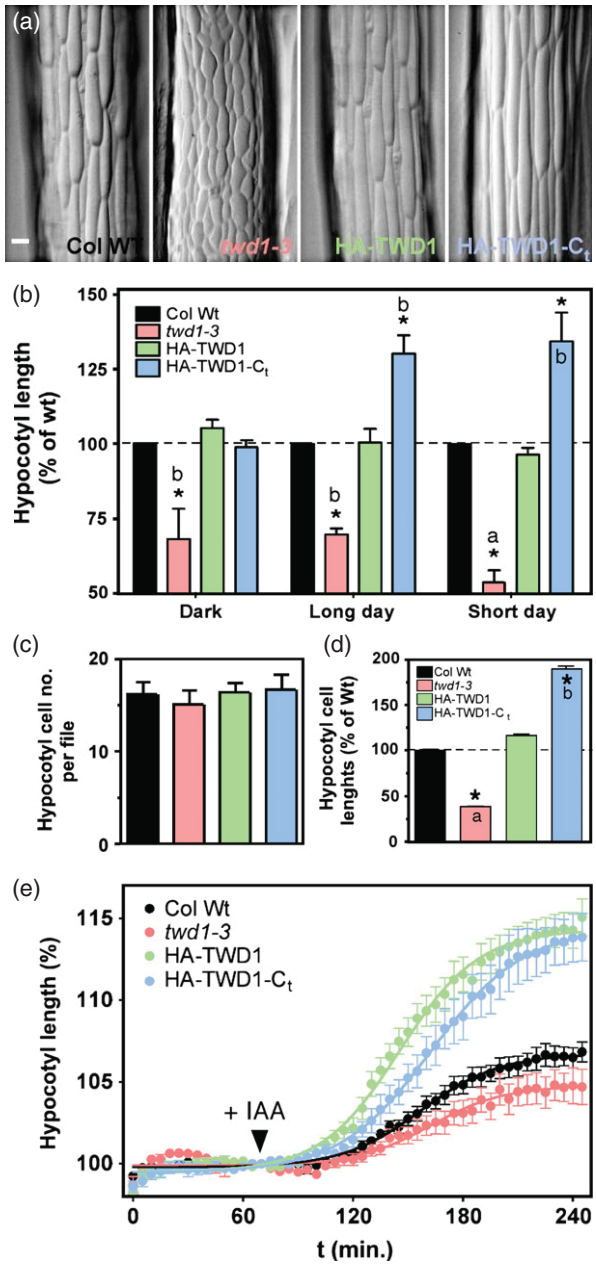

Figure 3. Hypermorphism of HA–TWD1-C_t plants is caused by enhanced cell elongation.
(a) Agarose imprints of Wt (Col Wt), *twd1-3*, HA–TWD1 and HA–TWD1-C_t lines under 8 h light conditions. Scale bar: 50 μm.
(b–d) Hypocotyl length (b), hypocotyl cell number (c) and cell length (d) of Wt (Col Wt), *twd1-3*, HA–TWD1 and HA–TWD1-C_t lines grown under indicated light conditions. Significant differences (ANOVA using the Tukey test for multiple comparisons: (a) $P < 0.01$; (b) $P < 0.05$) of means (± SE; $n = 6$) to Wt are indicated by asterisks.
(e) Hypocotyl elongation normalized to 100% at time point of addition of 100 nM IAA at $t = 70$ min. (arrow) of wild type (Col Wt), *twd1-3*, HA–TWD1 and HA–TWD1-C_t. Mean ± standard error (SE); $n = 14$.

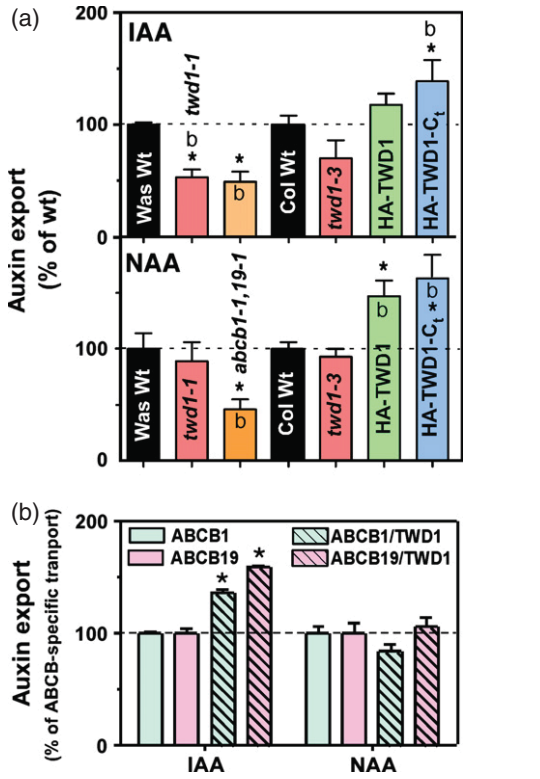

Figure 4. TWD1 positively controls cellular auxin and alters substrate specificity.
(a) Cellular auxin (IAA and NAA) efflux from Wt (Was Wt/Col Wt), *twd1-1, twd1-3, abcb1-1, b19-1*, HA–TWD1 and HA–TWD1-C_t leaf mesophyll protoplasts. Mean ± standard error (SE); $n = 4$–8. Note that diffusion background equal to de-energized export was calculated to be roughly 30%. Significant differences were determined by analysis of variance (ANOVA) using the Tukey test for multiple comparisons: (a) $P < 0.01$; (b) $P < 0.05$) of means ± SE; ($n = 6$) to the corresponding Wt are indicated by asterisks.
(b) TWD1 enhances ABCB1- and ABCB19-mediated IAA efflux but not of the synthetic auxin, NAA from yeast (*S. pombe*) cells. Mean ± SE; $n = 4$. Significant differences (ANOVA using the Tukey's test for multiple comparisons: $P < 0.05$) ± TWD1 are indicated by an asterisk.

In summary, these data generated in Arabidopsis and several heterologous systems verified the idea that TWD1 functions as a rate-limiting, positive modulator of ABCB-mediated auxin efflux, but indicated also a role as a specificity filter in an action that is not dependent on further plant-specific factors.

Enhanced cellular auxin efflux in *TWD1* gain-of-function alters PAT and auxin accumulation

We next assayed and imaged basipetal transport of *TWD1* gain- and loss-of-function lines in the root (shoot-ward) and shoot (root-ward) employing a range of methods. Using radiolabeled auxin tracers we found a reduction in basipetal PAT in the hypocotyl (root-ward) and the root (shoot-ward) using the *twd1-3* allele [Figure 5(a)]. Reductions of cell and hypocotyl length are in line with reduced cellular efflux rates using the *twd1-1* allele (Figure 3(b); Bouchard *et al.*, 2006; Wu *et al.*, 2010). Surprisingly, and in contrast with cellular efflux measurements, PAT was strongly inhibited in HA–TWD1-C_t hypocotyls and roots.

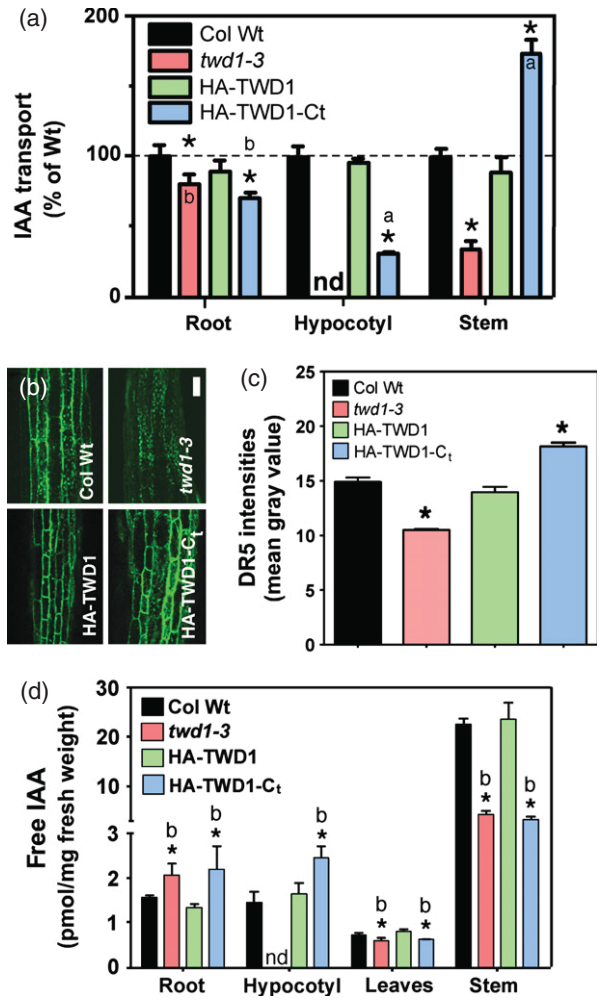

Figure 5. Genetic manipulation of *TWD1* expression alters shoot PAT and IAA levels.

(a) Basipetal root, hypocotyl and stem auxin transport of wild type (Col Wt), *twd1-3*, HA–TWD1 and HA–TWD1-C_t plants. For controls see Figures S4 and S5. nd; not determined.

(b, c) Confocal images (b) and quantification (c) of upper hypocotyl signals of the auxin-responsive reporter DR5::GFP (green) in wild type (Col Wt), *twd1-3*, HA–TWD1 and HA–TWD1-C_t. Mean intensities (gray value) ± standard error (SE); $n = 20$; Scale bar: 40 μm.

(d) Free IAA of wild type (Col Wt), *twd1-3*, HA–TWD1 and HA–TWD1-C_t roots, hypocotyls and leaves. Mean ± SE; $n = 4$ with each 40–50 seedlings. Significant differences were determined by analysis of variance (ANOVA) using the Tukey test for multiple comparisons: (a) $P < 0.01$; (b) $P < 0.05$) of means (± SE; $n = 8$) to Wt are indicated by asterisks.

However, these transport reductions, usually correlated with enhanced auxin levels in these tissues (Bouchard *et al.*, 2006; Bailly *et al.*, 2008), are obviously in accordance with reduced root- and enhanced hypocotyl lengths, respectively, found for HA–TWD1-C_t [Figure 3(b)].

Root and hypocotyl data did not directly explain the highly enhanced stem lengths and internode numbers. Therefore, we performed root-ward IAA transport assays in stems that showed highly enhanced transport for HA–TWD1-C_t that most probably accounts for hypermorphic stem sizes (Figure 1 and Table S2 online) and branching defects (Figure 2). Differences to the wild type were greatly enhanced at apical ends of the stems, correlated with younger, developing tissues (Matsuda *et al.*, 2011) and with higher auxin contents on one hand, and higher ABCB, primarily ABCB1, expression on the other hand [Figure S5 (b)]. Defects in stem transport was specific to IAA and was not the primary cause of altered stem architecture or diameter, as the diffusion control, BA, was not transported significantly differently from wild type (Figure S5). Moreover, a pulse-chase application with unlabeled IAA shifted IAA accumulation significantly in HA–TWD1-C_t but not in HA–TWD1 or in *twd1,* clearly demonstrating again that differences in auxin accumulation are the direct result of altered PAT (Figure S6).

In order to support these rather invasive PAT experiments and to enhance resolution, we performed analyses of root IAA responses using the auxin-responsive element DR5::GFP (Ottenschlager *et al.*, 2003). Judged by visual evaluation [Figure 5(b)] and computer-assisted quantification [Figure 5(c)] of confocal microscopy images, HA–TWD1 showed a slightly reduced, but comparable DR5::GFP expression in the hypocotyl to wild type. However, *twd1-3* and HA–TWD1-C_t hypocotyls showed significantly lower and higher DR5::GFP signals, respectively [Figure 5(b,c)] in comparison with the Wt. Additionally, DR5::GFP signals in *twd1-3* were limited to punctate structures partially also found in Wt, HA–TWD1 or HA–TWD1-C_t [Figure 5(b)].

Finally, we quantified free IAA in hypocotyls, roots and stem sections of *TWD1* gain-of-function lines by gas chromatography–mass spectrometry (GC–MS). Probably as a consequence of reduced basipetal transport capacities [Figure 5(a)], *twd1-3* and HA–TWD1-C_t seedlings showed enhanced accumulation of free IAA in their roots [Figure 5(d)]. This result was not found for cotyledons that in agreement (beside epinasty), but unlike true leaves, showed no obvious growth defects. Consistently with elongated hypocotyls, free IAA was also elevated in HA–TWD1-C_t hypocotyls, while preparation of sufficient material of *twd1-3* hypocotyls for IAA quantification was hindered by the growth phenotype [Figure 5(d)]. However, according to a report that demonstrated reduced free auxin for entire *twd1-1* shoots (= aerial parts; Bouchard *et al.*, 2006), one might predict that the same outcome holds true for hypocotyls thought to form essentially embryonic shoots. This assumption would be obviously in line with reduced *twd1* hypocotyl lengths [Figure 3(d)].

Interestingly, the tendency of elevated free IAA was not found in stem segments, which contained about 10 times more auxin compared with material prepared from seedlings. Free IAA in *twd1-3* and HA–TWD1-C_t was greatly reduced; the latter is obviously consistent with elevated stem IAA transport [Figure 5(a)].

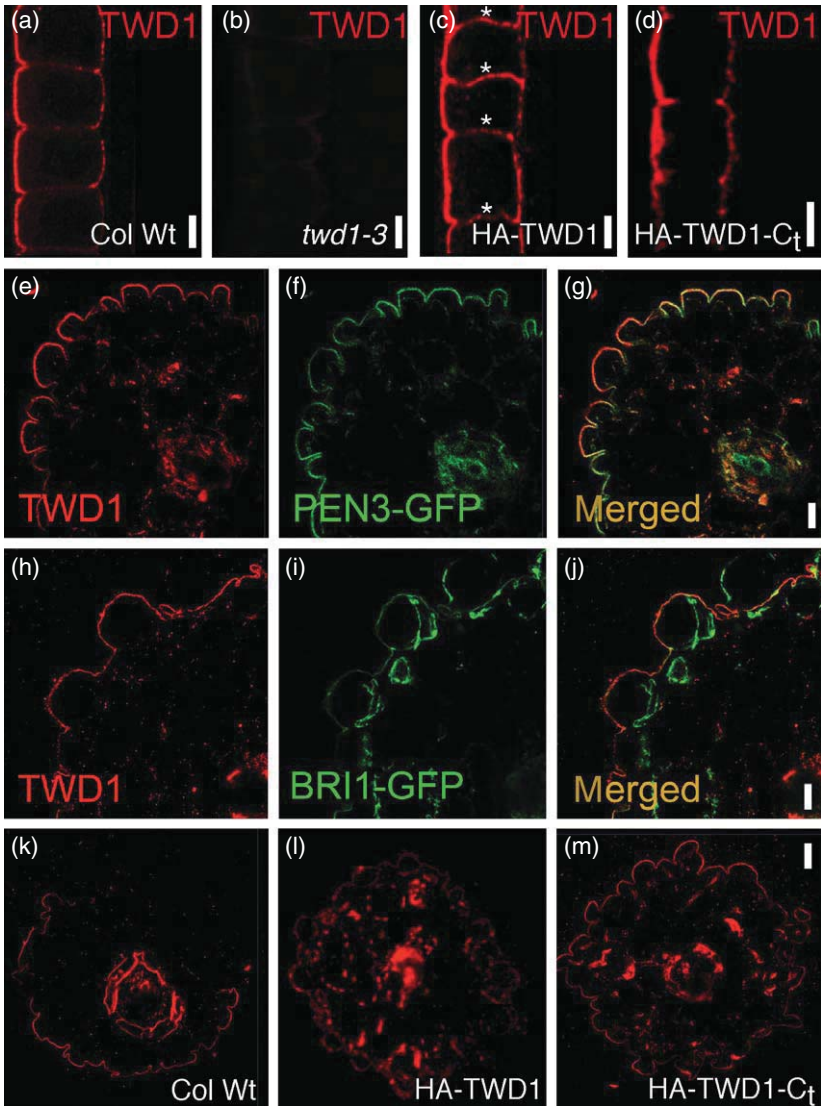

Figure 6. Whole-mount immunostaining reveals polar plasma membrane locations in the epidermis of roots and hypocotyl.
(a–d) Whole-mount immunostaining of a primary Wt root tip (a) with anti-TWD1, indicating predominant expression in the epidermis with a lateral (stronger at the outer polar domain) plasma membrane localization. Note the absence of signal in the *twd1-3* mutant (b), loss of polarity in HA–TWD1 (marked by asterisks; c) and up-regulation in HA–TWD1 and HA–TWD1-C_t (d). Scale bars: 20 μm.
(e–j) Whole-mount immunostaining using anti-TWD1 in PEN3–GFP (e–g) and BRI1–GFP (h–j) hypocotyl sections indicating predominant TWD1 expression in the epidermis with a lateral (stronger at the outer polar domain) plasma membrane localization. Note the wide colocalization with lateral marker PEN3 and only partial overlap with non-polar marker BRI1. Scale bars: 50 μm (e–g) and 20 μm (h–j).
(k–m) Whole-mount immunostaining of Wt (k), HA–TWD1 (l) and HA–TWD1-C_t (m) hypocotyl sections. Note the up-regulation and additional expression between epidermis and stele in HA–TWD1 and HA–TWD1-C_t. Scale bars: 75 μm.

In summary, these results employing radiolabeled IAA tracers, DR5::GFP imaging and quantification of free IAA provide evidence that both reduced/elevated cellular auxin efflux in *twd1*/HA–TWD1-C_t are the primary cause for defects in basipetal PAT leading to altered hypocotyl and stem auxin accumulation.

HA–TWD1-C_t shows a similar PM polarity as the wild-type protein

In a previous study, immunocytochemical analyses revealed that TWD1 resides on lateral PM domains with stronger labeling at the outward-facing side [Figure 6(a)] that perfectly matched that of the lateral PM marker PEN3/ABCG36-GFP (Wang *et al.*, 2013). Analyses of HA–TWD1 indicated an up-regulation, but also a partial loss, of lateral polarity resulting in additional labeling of basal and apical plasma membrane ends [Figure 6(c)], overall resembling 35S::TWD1-YFP expression (Wang *et al.*, 2013). This finding indicates that loss of polarity might be, at least partially, caused by over-expression. Reduced polarity of HA–TWD1 also gives rise, together with higher expression levels, to a mechanistic rationale for enhanced root bending kinetics (Bailly *et al.*, 2008; Wang *et al.*, 2013) reflected by wider root IAA influx peaks and enhanced basipetal DR5::GFP signals (Wang *et al.*, 2013).

Surprisingly, immunodetection of HA–TWD1-C_t that lacked the C-terminal membrane anchor resulted in a stronger but similar plasma membrane pattern to the wild type [Figure 6(d)]. However, the presence of both TWD1-OX at the PM was verified by western blot analysis of sucrose gradient fractions using anti-TWD1 and anti-HA and revealed that HA–TWD1 and HA–TWD1-C_t overlap with the PM markers plasma membrane-intrinsic protein and H^+-ATPase (Figure S7). Both HA–TWD1 and HA–TWD1-C_t detected by anti-HA also partially overlapped with the ER marker binding Protein although at reduced molecular

weight consistent with a previously published ER location (Wu *et al.*, 2010; Wang *et al.*, 2013). These data are in line with previous results in yeast that demonstrated that even the soluble TWD1 FKBD was fully competent in regulating ABCB1 activity and membrane-bound in the presence but not in the absence of ABCB1 (Bailly *et al.*, 2008).

In order to further substantiate the root-derived TWD1 localization data and to better relate them to described shoot phenotypes, we repeated anti-TWD1 immunolocalization in hypocotyl cross-sections. Analogous to the root data, we found polar, mainly outward-facing, signals for TWD1 that were limited to the epidermis, although with less polarity [Figure 6(e)]. In these tissues, TWD1 widely overlapped the lateral marker, PEN3-GFP, and partially with non-polar marker, BRI1-GFP, but only on its lateral domains [Figure 6(e–g)]. Interestingly, as in the root epidermis, TWD1-OX showed stronger expression in general and also in ectopic expression in the cortex between epidermis and stele [Figure 6(k–m)]. Moreover, HA–TWD1 revealed reduced polarity as found in the root.

DISCUSSION

The hypermorphic phenotype of HA–TWD1-C_t is caused by altered polar auxin transport

In this work we report that constitutive over-expression of HA–TWD1-C_t leads to a hypermorphic phenotype characterized predominantly by enhanced stem length and leaf surface (Figure 1) but reduced shoot branching (Figure 2). Branching defects are in line with altered IAA contents (Figure 5) that might change concentrations of strigolactone in the stem. This aspect is currently under investigation but strigolactone was shown to control shoot branching by reducing auxin transport from axillary buds (Gomez-Roldan *et al.*, 2008). Further, we show that HA–TWD1-C_t shoot hypermorphism is caused by highly increased cell length that is a direct result of enhanced IAA-dependent tissue elongation as exemplified here for the hypocotyl (Figure 3). Finally, we demonstrate that enhanced IAA-dependent cell elongation is most probably the direct consequence of altered polar auxin transport capacities caused by expression of HA–TWD1-C_t.

Interestingly, in the hypocotyl enhanced cellular auxin export capacities in HA–TWD1-C_t as measured using isolated protoplasts (Figure 4) resulted in strongly reduced basipetal auxin reflux that caused elevated auxin accumulation, as judged by tracking radiolabeled IAA movement and DR5::GFP imaging (Figure 5). As a consequence, HA–TWD1-C_t displayed elevated hypocotyl levels of free auxin (Figure 5). This finding is in agreement with enhanced shoot cell elongation and size (Figures 1 and 3) and led finally to a 'giant' shoot phenotype in the adult plant. This outcome was demonstrated by means of hypocotyl elongation assays in which, upon addition of IAA, both TWD1-OX alleles revealed highly enhanced hypocotyl elongation kinetics (Figure 3). Surprisingly, the difference between HA–TWD1 and HA–TWD1-C_t is only marginal in these elongation experiments as well as in cellular efflux (protoplast) assays, a finding that is in contrast with the *in vivo* measurements (see Figure 3(a) and Table S3). This difference is probably caused by the fact that in these '*in vitro*' assays, excised hypocotyl segments or isolated protoplasts have lost their tissue context or their cell polarity, respectively, and therefore have to be – despite their individual value – interpreted with care.

It should also be mentioned that hypocotyl and stem PAT capacities are inversely affected in HA–TWD1-C_t [Figure 5(a)], although quantification of DR5::GFP expression and of free IAA are in perfect agreement, respectively (see Table S3). The simplest explanation is that TWD1 (and as such also HA–TWD-C_t) can have inverse effects on ABCB-mediated auxin transport in different tissues and developmental stages. The first effect is supported by a row of heterologous expression analyses using several yeast and plant systems that indicate that TWD1 is able to stimulate, but also block, ABCB transport (Bouchard *et al.*, 2006; Bailly *et al.*, 2008; Henrichs *et al.*, 2012; this work). This phenomenon is not fully understood but seems to be, at least in part, dependent on differential ABCB linker phosphorylation provided by the AGC kinase, PINOID (Henrichs *et al.*, 2012). Moreover, analogous to the mammalian TWD1 ortholog, FKBP38, other third-party TWD1-interacting proteins (such as calmodulin and HSP90; Geisler and Bailly, 2007; Kamphausen *et al.*, 2002), that each were shown to have inverse effects on FKP38 functionality, might also modulate TWD1 activity. These data however also indicate that it is an over-simplification to consider hypocotyls as 'embryonic stems'.

In summary, most phenotypical and physiological analyses reveal that HA–TWD1-C_t behaves oppositely to *twd1*, while HA–TWD1 complements the loss-of-function mutant widely to wild-type levels (see Table S3 for an overview). However, a few indicated discrepancies also reflect that the action of TWD1 on ABCB activity is not as simple as it looks and is highly tissue-specific. As molecular reasons, besides the above-mentioned, for this likely concept that TWD1 itself might have positive and negative impacts on ABCBs (Henrichs *et al.*, 2012), it should be re-emphasized that TWD1 regulates, beside ABCB1 at minimum, also the two closely related ABCB isoforms ABCB19 and ABCB4 (Wang *et al.*, 2013; Wu *et al.*, 2010). These homologs were independently shown to be involved in opposite PAT streams (Geisler *et al.*, 2005; Bouchard *et al.*, 2006; Wu *et al.*, 2007; Cho and Cho, 2012). Therefore, dependent on their expression profile, one might imagine a scenario in which, depending on the presence of TWD1 and additional regulatory co-factors, TWD1 functions as an integrator of PAT streams.

In many aspects, HA–TWD1-C_t lines resemble the auxin overproduction phenotypes of *YUCCA6* over-expressing lines that show long hypocotyls and extremely tall unbranched inflorescences (Kim *et al.*, 2007) but epinastic cotyledons like twd1 (Geisler *et al.*, 2003). Moreover, as with *YUCCA6-OX,* HA–TWD1-C_t lacks a short root phenotype and morphological changes under dark conditions (Kim *et al.*, 2007; Wang *et al.*, 2013). Interestingly, HA–TWD1-C_t revealed enhanced seed size, but not circularity after water imbibing, another trait of the *YUCCA6* dominant mutation that was also found for *b19*, *b1 b19* and *twd1* but not *HA–TWD1* seeds (Figure S3); this finding supports the idea that hypermorphic phenotypes are the result of enhanced auxin levels.

Interestingly, the fact that higher cell elongation rates for HA–TWD1-C_t hypocotyls were only found in the light resembles light-dependent root length inhibition in the dark (Wang *et al.*, 2013) and argues for an involvement of TWD1 in light-dependent development. This scenario has been previously suggested in a study that described the regulation of B19 by the AGC kinase, phot1 (Christie *et al.*, 2011). TWD1–ABCB19 interaction was improved by light irradiation but enhanced in *phot1* loss-of-function plants, supporting the concept that phot1-catalysed ABCB19 phosphorylation blocks TWD1–ABCB19 interaction (Christie *et al.*, 2011; Christie and Murphy, 2013).

Finally, our data support a role of TWD1 in controlling lateral export of IAA by ABCBs into the epidermal apoplast that is required for the activation of essential processes of cell elongation, including cell-wall loosening and apoplastic acidification via activation of the PM H^+-ATPase (Christian *et al.*, 2006). In that respect our findings link very recent findings on the auxin-induced activation of the proton pump (Takahashi *et al.*, 2012) with the proposed role of auxin in frame of the original acid growth theory (Rayle and Cleland, 1970, 1992). Our data are also in agreement with models that suggest that the auxin-efflux transporter complex itself possesses an auxin receptor function (Zhao *et al.*, 2002; Hossel *et al.*, 2005).

However, the finding that laterally expressed HA–TWD1-C_t, but not apolar TWD1-HA (Figure 6), shows enhanced longitudinal hypocotyl cell elongation is indirect proof of the concept for the role of lateral auxin distribution into the apoplast in this process (Wang *et al.*, 2013).

Removal of the TWD1 membrane anchor supports a primary function of TWD1 in ABCB biogenesis in analogy to human FKBP38

The discrepancy in phenotype and most of the employed physiological assays between HA–TWD1 and HA–TWD1-C_t both expressed under the same promoter in the mutant background argues, therefore, for an essential role of the IPM anchor in HA–TWD1-C_t functionality (Scheidt *et al.*, 2007).

Crucial relevance of the IPM is analogous to FKBP38 function, the closest human TWD1 ortholog, acting as a negative regulator of apoptosis on the mitochondria outer-membrane (Shirane and Nakayama, 2003) and as a positive regulator of PM anion channel biogenesis on the ER membrane (Banasavadi-Siddegowda *et al.*, 2011). Regulation of CFTR, an ABCC/MRP-type ABC transporter primarily functioning as a chloride channel (Gadsby *et al.*, 2006), is of special interest because FKBP38 promotes CFTR post-translational folding through its PPIase activity but inhibits CFTR protein synthesis through its membrane anchorage (Banasavadi-Siddegowda *et al.*, 2011). Although all attempts to monitor a TWD1 PPIase activity have failed so far (Kamphausen *et al.*, 2002; Geisler *et al.*, 2003), it is tempting to speculate that an analogous function might hold true for TWD1, especially in light of the functional interaction with CFTR-related ABCC1/MRP1 and ABCC2/MRP2 on the tonoplast (Geisler *et al.*, 2004).

This structural and functional analogy suggests that the principal role of TWD1 might be close to its FKBP38 ortholog in mediating ABCB folding at the cytoplasmic ER surface (Wu *et al.*, 2010) and that its interaction with ABCBs at the plasma membrane recently described in Wang *et al.* (2012) might be secondary. However, in contrast with TWD1, absence of the FKBP38 membrane anchor leads to FKBP38 mis-targeting and subsequent apoptosis (Shirane and Nakayama, 2003), while heterologous expression of a truncated version of FKBP38 abolishes its inhibition of CFTR synthesis but does influence its role in post-translational folding. In light of the growth promoting phenotype of HA–TWD1-C_t, we believe that the functional role of the TWD1 IPM might be slightly distinct as its deletion promotes apparently TWD1 functionality. As such the most logical explanation is that the IPM anchor keeps TWD1 at the PM and thus interferes with its primary function in a putative shuttling from the ER to the PM. This is indirectly supported by yeast experiments showing that even the soluble FKBD of TWD1 was membrane-associated in the presence but not in the absence of co-expressed ABCB1 (Bailly *et al.*, 2008). Moreover, yeast FKBP12 consisting essentially of the TWD1 FKBD, was recently shown to complement *TWD1* loss of-function mutants (Henrichs *et al.*, 2012), providing evidence that, in contrast with FKBP38, the FKBD has a prominent function in ABCB regulation.

EXPERIMENTAL PROCEDURES

Plant material and phenotypic analyses

Analogous to HA–TWD1 (Geisler *et al.*, 2003), for HA–TWD1-C_t constructs, the 9-aa-long HA-tag was fused genetically to amino

acids 1–337 and inserted into the binary vector pGPTV-KAN. The resulting binary construct was used to transform Arabidopsis *twd1-3* via vacuum infiltration and several independent, homozygous lines were generated. *abcb1-1/pgp1-1* (At2 g36910), *abcb19-1/pgp19-1/mdr1-1* (At3 g28860), *twd1-1* (At3 g21649; all ecotype Wassilewskija) and *twd1-3* (ecotype Columbia) were grown on vertical plates containing 0.5 × Murashige and Skoog (MS) medium, 1% sucrose, 0.7% phytagar in the dark or at 8 h (short-day), 16 h (long-day) or 24 h (constant) light per day. Growth parameters were quantified as in Kim *et al.* (2010). A detailed phenotypical and developmental analysis of *twd1-3*, HA–TWD1 and HA–TWD1-C_t was carried out as in Boyes *et al.* (2001).

Orientation of epidermal layers (angles to the growth direction) was quantified microscopically using agarose imprints (Weigel and Glazebrook, 2009). Root gravitropism and hypocotyl elongation was analyzed as in Bailly *et al.* (2008) and Schenck *et al.* (2010), respectively. All experiments were performed at least in triplicate with 30–50 seedlings per each experiment.

Auxin transport assays

Yeast IAA and NAA transport was assayed with the unspecific BA as control in parallel and performed as in Bailly *et al.* (2008) and Kim *et al.* (2010). Relative export is calculated from retained radioactivity as follows: (radioactivity in the yeast at time t = 10 min) − (radioactivity in the yeast at time t = 0) × (100%)/(radioactivity in the yeast at t = 0 min). IAA export from Arabidopsis mesophyll protoplasts was analyzed as in Henrichs *et al.* (2012) and polar auxin transport was assayed as in Lewis and Muday (2009). The values presented are mean values from 6–8 independent experiments.

Localization analysis and confocal microscopy

Immunolocalizations in 5-day-old seedlings were carried out as described in Wang *et al.* (2013) with anti-TWD1 (1:500), anti-PIN1,2 (1:500) and Cy3-conjugated anti-rabbit (1:600; Dianova) antibodies. Additional constructs and lines were: PEN3/ABCG36-GFP (Stein *et al.*, 2006), ABCB1– and B19–GFP (Mravec *et al.*, 2008). For confocal laser scanning microscopy, Leica TCS SP2, Leica TCS SP5 or Leica DMIRE2 equipment were used.

Analysis of IAA contents

Endogenous free IAA was quantified from root, hypocotyl and cotyledon segments of MeOH extracted seedlings by using GC–MS as described in Bouchard *et al.* (2006). Data are the means of four independent lots of 30–50 seedlings each grown on independent plates.

DR5::GFP (Ottenschlager *et al.*, 2003) signals in Arabidopsis upper hypocotyls grown under 8 h light condition were observed 3 days after germination (dag) as described in Bailly *et al.* (2008).

Data analysis

Data were analyzed using Prism 5.0 (GraphPad Software, San Diego, CA). Confocal images were images were processed in Adobe Photoshop 10.0.1. (Adobe Systems, Mountain View, CA) and quantified using ImageJ 1.43 with the original TIFF files pixel brightness threshold set to a minimum of 25.

ACKNOWLEDGEMENTS

We would like thank V. Vincenzetti, L. Charrier and P. Düchting for excellent technical assistance, T. Buchala for comments on the text, M. B. Palmgren for discussion and support and E. Martinoia for support and mentorship. This work was supported by grants from the European Social Fund (CZ.1.07/2.3.00/20.0043) and the Czech Science Foundation GAČR (GA13-40637S) to JF; project "Postdoc I." (CZ.1.07/2.3.00/30.0009) co-financed by the state budget of the Czech Republic to MZ. Part of work was realized in the CEITEC – Central European Institute of Technology (CZ.1.05/1.1.00/02.0068), Novartis Foundation (to M.G.), from the Danish Research School for Biotechnology, FOBI (to M.G. and A.S.), from the Forschungskredit of the University of Zurich (to A.B.), from the *Pol de Recherche* of the University of Fribourg (to M.G.) and from the Swiss National Funds (to M.G.)

AUTHOR CONTRIBUTIONS

M.G. and A.B. designed the research; R.B., A.B., B.W. and M.G. performed auxin transport analyses; A.B. created HA–TWD1-C_t lines and analyzed hypocotyl elongation and shoot branching; A.B. and B.W. analyzed DR5::GFP expression and plant phenotypes; D.S. and H.L. carried out hypocotyl elongation assays; S.P. analyzed free auxins; M.Z. and J.F. performed TWD1 ILs and A.S., A.B. and M.G. wrote the manuscript.

SUPPORTING INFORMATION

Additional Supporting Information may be found in the online version of this article.

Figure S1. HA–TWD1-C_t rosettes are bushier than Wt (Col Wt), *twd1* (*twd1-3*) or HA–TWD1 grown for 40 dag under 8 h light caused by an elevated number of rosette leaves.

Figure S2. Light fluence-dependency of root (A–B) and hypocotyl length (C–D) of wild-type (Col0), *twd1* (*twd1-3*), HA–TWD1 or HA–TWD1-C_t lines under short-day (8 h light) and long-day (16 h light) conditions.

Figure S3. Seed size and circularity of *TWD1* and *ABCB* mutant alleles.

Figure S4. TWD1 inhibits ABCB1-mediated IAA efflux but not of synthetic auxin, NAA, or of specificity control, benzoic acid (BA) from the yeast, *S. cerevisiae*.

Figure S5. Basipetal transport of IAA in TWD1 loss- and gain-of-function stems.

Figure S6. Pulse-chase transport of IAA in *TWD1* loss- and gain-of-function stems.

Figure S7. Separation of TWD1 gain-of-function microsomes using discontinuous sucrose gradient centrifugation.

Table S1. Phenotypic analysis of wild-type (Col Wt), *twd1-3*, HA–TWD1 and HA–TWD1-C_t plants grown under long-day (16 h light) and short-day (8 h light) conditions until growth stage 1 (Boyes *et al.*, 2001).

Table S2. Phenotypic analysis of wild type (Col Wt), *twd1-3*, HA–TWD1 and HA–TWD1-C_t plants grown under long-day (16 h light) and short-day (8 h light) conditions starting with growth stage 1 (Boyes *et al.*, 2001).

Table S3. Summary of morphological and physiological parameters measured in this study.

REFERENCES

Bailly, A., Sovero, V., Vincenzetti, V., Santelia, D., Bartnik, D., Koenig, B.W., Mancuso, S., Martinoia, E. and Geisler, M. (2008) Modulation of P-glycoproteins by auxin transport inhibitors is mediated by interaction with immunophilins. *J. Biol. Chem.* **283**, 21817–21826.

Banasavadi-Siddegowda, Y.K., Mai, J., Fan, Y., Bhattacharya, S., Giovannucci, D.R., Sanchez, E.R., Fischer, G. and Wang, X. (2011) FKBP38

peptidylprolyl isomerase promotes the folding of cystic fibrosis transmembrane conductance regulator in the endoplasmic reticulum. *J. Biol. Chem.* **286**, 43071–43080.

Bennett, T. and Scheres, B. (2010) Root development-two meristems for the price of one? *Curr. Top. Dev. Biol.* **91**, 67–102.

Bouchard, R., Bailly, A., Blakeslee, J.J. *et al.* (2006) Immunophilin-like TWISTED DWARF1 modulates auxin efflux activities of Arabidopsis P-glycoproteins. *J. Biol. Chem.* **281**, 30603–30612.

Boyes, D.C., Zayed, A.M., Ascenzi, R., McCaskill, A.J., Hoffman, N.E., Davis, K.R. and Gorlach, J. (2001) Growth stage-based phenotypic analysis of Arabidopsis: a model for high throughput functional genomics in plants. *Plant Cell*, **13**, 1499–1510.

Braun, N., Wyrzykowska, J., Muller, P., David, K., Couch, D., Perrot-Rechenmann, C. and Fleming, A.J. (2008) Conditional Repression of AUXIN BINDING PROTEIN1 Reveals That It Coordinates Cell Division and Cell Expansion during Postembryonic Shoot Development in Arabidopsis and Tobacco. *Plant Cell*, **20**, 2746–2762.

Cho, M. and Cho, H.T. (2012) The function of ABCB transporters in auxin transport. *Plant Signal. Behav.* **8**, e22990.

Christian, M., Steffens, B., Schenck, D., Burmester, S., Bottger, M. and Luthen, H. (2006) How does auxin enhance cell elongation? Roles of auxin-binding proteins and potassium channels in growth control. *Plant Biol (Stuttg).* **8**, 346–352.

Christie, J.M. and Murphy, A.S. (2013) Shoot phototropism in higher plants: new light through old concepts. *Am. J. Bot.* **100**, 35–46.

Christie, J.M., Yang, H., Richter, G.L. *et al.* (2011) phot1 inhibition of ABCB19 primes lateral auxin fluxes in the shoot apex required for phototropism. *PLoS Biol.* **9**, e1001076.

Gadsby, D.C., Vergani, P. and Csanady, L. (2006) The ABC protein turned chloride channel whose failure causes cystic fibrosis. *Nature*, **440**, 477–483.

Geisler, M. and Bailly, A. (2007) Tete-a-tete: the function of FKBPs in plant development. *Trends Plant Sci.* **12**, 465–473.

Geisler, M. and Henrichs, S. (2013). Regulation of polar auxin transport by protein-protein interactions. In *Signaling and Communication in Polar Auxin Transport* (Chen, R. and Baluška, F., eds). Berlin: Springer-Verlag, pp. 155–178.

Geisler, M. and Murphy, A.S. (2006) The ABC of auxin transport: the role of p-glycoproteins in plant development. *FEBS Lett.* **580**, 1094–1102.

Geisler, M., Kolukisaoglu, H.U., Bouchard, R. *et al.* (2003) TWISTED DWARF1, a unique plasma membrane-anchored immunophilin-like protein, interacts with Arabidopsis multidrug resistance-like transporters AtPGP1 and AtPGP19. *Mol. Biol. Cell*, **14**, 4238–4249.

Geisler, M., Girin, M., Brandt, S. *et al.* (2004) Arabidopsis immunophilin-like TWD1 functionally interacts with vacuolar ABC transporters. *Mol. Biol. Cell*, **15**, 3393–3405.

Geisler, M., Blakeslee, J.J., Bouchard, R. *et al.* (2005) Cellular efflux of auxin catalyzed by the Arabidopsis MDR/PGP transporter AtPGP1. *Plant J.* **44**, 179–194.

Gomez-Roldan, V., Fermas, S., Brewer, P.B. *et al.* (2008) Strigolactone inhibition of shoot branching. *Nature*, **455**, 189–194.

Hager, A. (2003) Role of the plasma membrane H + -ATPase in auxin-induced elongation growth: historical and new aspects. *J. Plant. Res.* **116**, 483–505.

Henrichs, S., Wang, B., Fukao, Y. *et al.* (2012) Regulation of ABCB1/PGP1-catalysed auxin transport by linker phosphorylation. *EMBO J.* **31**, 2965–2980.

Hossel, D., Schmeiser, C. and Hertel, R. (2005) Specificity patterns indicate that auxin exporters and receptors are the same proteins. *Plant Biol (Stuttg).* **7**, 41–48.

Jensen, P.J., Hangarter, R.P. and Estelle, M. (1998) Auxin transport is required for hypocotyl elongation in light-grown but not dark-grown Arabidopsis. *Plant Physiol.* **116**, 455–462.

Kamphausen, T., Fanghanel, J., Neumann, D., Schulz, B. and Rahfeld, J.U. (2002) Characterization of *Arabidopsis thaliana* AtFKBP42 that is membrane-bound and interacts with Hsp90. *Plant J.* **32**, 263–276.

Kim, J.I., Sharkhuu, A., Jin, J.B. *et al.* (2007) yucca6, a dominant mutation in Arabidopsis, affects auxin accumulation and auxin-related phenotypes. *Plant Physiol.* **145**, 722–735.

Kim, J.Y., Henrichs, S., Bailly, A., Vincenzetti, V., Sovero, V., Mancuso, S., Pollmann, S., Kim, D., Geisler, M. and Nam, H.G. (2010) Identification of an ABCB/P-glycoprotein-specific inhibitor of auxin transport by chemical genomics. *J. Biol. Chem.* **285**, 23309–23317.

Lewis, D.R. and Muday, G.K. (2009) Measurement of auxin transport in *Arabidopsis thaliana*. *Nat. Protoc.* **4**, 437–451.

Matsuda, S., Kajizuka, T., Kadota, A., Nishimura, T. and Koshiba, T. (2011) NPH3- and PGP-like genes are exclusively expressed in the apical tip region essential for blue-light perception and lateral auxin transport in maize coleoptiles. *J. Exp. Bot.* **62** 3459–3466.

Mravec, J., Kubes, M., Bielach, A., Gaykova, V., Petrasek, J., Skupa, P., Chand, S., Benkova, E., Zazimalova, E. and Friml, J. (2008) Interaction of PIN and PGP transport mechanisms in auxin distribution-dependent development. *Development*, **135**, 3345–3354.

Ottenschlager, I., Wolff, P., Wolverton, C., Bhalerao, R.P., Sandberg, G., Ishikawa, H., Evans, M. and Palme, K. (2003) Gravity-regulated differential auxin transport from columella to lateral root cap cells. *Proc. Natl Acad. Sci. USA*, **100**, 2987–2991.

Petrasek, J., Mravec, J., Bouchard, R. *et al.* (2006) PIN proteins perform a rate-limiting function in cellular auxin efflux. *Science*, **312**, 914–918.

Rayle, D.L. and Cleland, R. (1970) Enhancement of wall loosening and elongation by Acid solutions. *Plant Physiol.* **46**, 250–253.

Rayle, D.L. and Cleland, R.E. (1992) The Acid Growth Theory of auxin-induced cell elongation is alive and well. *Plant Physiol.* **99**, 1271–1274.

Robert, H.S. and Friml, J. (2009) Auxin and other signals on the move in plants. *Nat. Chem. Biol.* **5**, 325–332.

Scheidt, H.A., Vogel, A., Eckhoff, A., Koenig, B.W. and Huster, D. (2007) Solid-state NMR characterization of the putative membrane anchor of TWD1 from *Arabidopsis thaliana*. *Eur. Biophys. J.* **36**, 393–404.

Schenck, D., Christian, M., Jones, A. and Luthen, H. (2010) Rapid auxin-induced cell expansion and gene expression: a four-decade-old question revisited. *Plant Physiol.* **152**, 1183–1185.

Shirane, M. and Nakayama, K.I. (2003) Inherent calcineurin inhibitor FKBP38 targets Bcl-2 to mitochondria and inhibits apoptosis. *Nat. Cell Biol.* **5**, 28–37.

Sidler, M., Hassa, P., Hasan, S., Ringli, C. and Dudler, R. (1998) Involvement of an ABC transporter in a developmental pathway regulating hypocotyl cell elongation in the light. *Plant Cell*, **10**, 1623–1636.

Stein, M., Dittgen, J., Sanchez-Rodriguez, C., Hou, B.H., Molina, A., Schulze-Lefert, P., Lipka, V. and Somerville, S. (2006) Arabidopsis PEN3/PDR8, an ATP binding cassette transporter, contributes to nonhost resistance to inappropriate pathogens that enter by direct penetration. *Plant Cell*, **18**, 731–746.

Takahashi, K., Hayashi, K. and Kinoshita, T. (2012) Auxin activates the plasma membrane H + -ATPase by phosphorylation during hypocotyl elongation in Arabidopsis. *Plant Physiol.* **159**, 632–641.

Teper-Bamnolker, P. and Samach, A. (2005) The flowering integrator FT regulates SEPALLATA3 and FRUITFULL accumulation in Arabidopsis leaves. *Plant Cell*, **17**, 2661–2675.

Vanneste, S. and Friml, J. (2009) Auxin: a trigger for change in plant development. *Cell*, **136**, 1005–1016.

Wang, B., Henrichs, S. and Geisler, M. (2012) The AGC kinase, PINOID, blocks interactive ABCB/PIN auxin transport. *Plant Signal. Behav.* **7**, 1515–1517.

Wang, B., Bailly, A., Zwiewka, M., Henrichs, S., Azzarello, E., Mancuso, S., Maeshima, M., Friml, J., Schulz, A. and Geisler, M. (2013) Arabidopsis TWISTED DWARF1 Functionally Interacts with Auxin Exporter ABCB1 on the Root Plasma Membrane. *Plant Cell*, **1**, 2012–2014.

Weigel, D. and Glazebrook, J. (2009) Phenotypic analysis of Arabidopsis mutants: bacterial pathogens. *Cold Spring Harb. Protoc.* **2009**. doi: 10.1101/pdb.prot4983.

Wu, G., Lewis, D.R. and Spalding, E.P. (2007) Mutations in Arabidopsis multidrug resistance-like ABC transporters separate the roles of acropetal and basipetal auxin transport in lateral root development. *Plant Cell*, **19**, 1826–1837.

Wu, G., Otegui, M.S. and Spalding, E.P. (2010) The ER-localized TWD1 immunophilin is necessary for localization of multidrug resistance-like proteins required for polar auxin transport in Arabidopsis roots. *Plant Cell*, **22**, 3295–3304.

Yang, H. and Murphy, A.S. (2009) Functional expression and characterization of Arabidopsis ABCB, AUX 1 and PIN auxin transporters in Schizosaccharomyces pombe. *Plant J.* **59**, 179–191.

Zhao, H., Hertel, R., Ishikawa, H. and Evans, M.L. (2002) Species differences in ligand specificity of auxin-controlled elongation and auxin transport: comparing Zea and Vigna. *Planta*, **216**, 293–301.